# SANDIA REPORT

SAND2018-6538
Unlimited Release
Printed May 2018

# The Effects of Stochastic Velocity Variations on Estimating Time Dependent Seismic Moment Tensors: Applications to the Blue Mountain Well Perforation Data

Christian Poppeliers and Leiph Preston

Prepared by
Sandia National Laboratories
Albuquerque, New Mexico 87185 and Livermore, California 94550

Sandia National Laboratories is a multimission laboratory managed and operated by National Technology and Engineering Solutions of Sandia, LLC., a wholly owned subsidiary of Honeywell International, Inc., for the U.S. Department of Energy's National Nuclear Security Administration under contract DE-NA0003525.



Sandia National Laboratories

Issued by Sandia National Laboratories, operated for the United States Department of Energy by National Technology and Engineering Solutions of Sandia, LLC.



SAND2018-6538
Unlimited Release
Printed May 2018

# The Effects of Stochastic Velocity Variations on Estimating Time Dependent Seismic Moment Tensors: Applications to the Blue Mountain Well Perforation Data

Christian Poppeliers
Geophysics Department
Sandia National Laboratories
P.O. Box 5800
Albuquerque, NM 87185-9999
cpoppel@sandia.gov

Leiph Preston
Geophysics Department
Sandia National Laboratories
P.O. Box 5800
Albuquerque, NM 87185-9999
lpresto@sandia.gov

**Abstract**

Resolving the time dependent terms in the seismic moment tensor provides important information that can be used to interpret the source process of an explosion, including the separation of isotropic explosion terms from shear forces and potentially isolated force couples. In this report, we detail our method of inverting three component seismic data for the seismic moment tensor. We review possible seismic source models from the simplest isotropic explosion type source to those incorporating the six independent moment tensor terms. The inversion we describe is formulated in the frequency domain, and results in estimates of time dependent moment tensor components.

The inversion relies on an accurate estimate of the Green's functions of the Earth. However, given the complexity of the Earth, we explore the effects of inaccuracies in the presumed Earth model used to estimate the Green's functions needed for the inversion. Specifically, we explore the effects of stochastic variations in the Earth models on the inversion results. These tests are synthetic throughout, and show that adding stochastic density/velocity heterogeneity in the presumed

Earth model results in reduced amplitude seismic moment tensor estimates, as well as degrading the data misfit. We suggest two mitigation strategies. First, produce a suite of Green's functions using different realizations of the stochastic field within the Earth Model. Secondly, perform the inversion in the power spectral domain, eliminating all phase information. Finally, we analyze actual seismic data collected in winter 2017/2018. The seismic data was collected at in active geothermal well site outside of Winnimucca, NV, and was produced during well stimulation operations. In general, the inversion results were poor, with a high degree of data misfit. We hypothesize that the poor results are a function of a poorly constrained Earth model as well as noisy, high-frequency data being used in the inversion.

# Acknowledgment

The authors acknowledge the National Nuclear Security Administration, Defense Nuclear Nonproliferation Research and Development (DNN R&D). Sandia National Laboratories is a multimission laboratory managed and operated by National Technology and Engineering Solutions of Sandia LLC, a wholly owned subsidiary of Honeywell International Inc. for the U.S. Department of Energy's National Nuclear Security Administration under contract DE-NA0003525.

# Contents

# List of Figures

# List of Tables

# Chapter 1

# Introduction

Inverting seismic data for the linear-equivalent source time function is a useful tool for understanding the mechanisms of the seismic source. For example, using an estimate of the equivalent seismic source, its possible to differentiate between an explosive seismic source and an earthquake, or determine the partitioning of energy from explosive sources. For example, the generation of shear-wave energy from an explosive source can be quantified by inverting for the seismic moment tensor, giving insights into a region's ability to scatter seismic energy, or background tectonic stresses, among other things (e.g. Yang and Bonner, 2009).

We developed an inverse scheme based on the assumption that the observed seismic data is a convolution of the seismic moment tensor with the appropriate Green's function which describes the impulse response of a given source type from the source location to the observing receiver. We also completely generalize the seismic moment tensor such that we assume that the source contains six independent terms and that each term in the moment tensor can have an independent, time domain representation, which we refer to as the time dependent moment tensor (TDMT).

Although time-domain seismic moment tensor inversions are not new, we developed our scheme for the purpose of investigating the effects of stochastic velocity variation in the geophysical models when inverting for the TDMT. Specifically, an inversion for seismic moment tensors must make use of a forward model used to predict the data. In this context, the forward model is a set of Green's functions that describe the impulse response of the model to a given source type at the source location to the observing receiver. The Green's function can be estimated using a geologic model, which implies that the accuracy of the geologic model can influence the inversion results. Typically, geologic models used to construct Green's functions are obtained via other geophysical methods, such as seismic refraction tomography or body wave tomography. These methods are biased towards smooth models as they only attempt to fit seismic arrival times without regard for frequency-dependent seismic wave scattering. However, it's well known that the Earth's crust, especially crystalline rocks are highly heterogeneous. In this case, a seismic wave field will scatter, rendering Green's function estimation highly problematic. One of our goals here is to explore the relative sensitivity of TDMT inversions in the presence of a highly scattering crust. Our approach presumes that the Earth is heterogeneous and that it can be described as an effective stochastic medium. For example, there have been several schemes to statistically characterize the heterogeneity of the Earth using equivalent statistical descriptions (e.g. Holliger and Levander, 1992, 1994; Levander et. al, 1994a,b). These methods use an effective statistical model to generate a stochastic velocity field that mimic, in a statistical sense, the actual deterministic features in the

crust. The success of these methods is noted by the similarity of modeled seismic waves through these models to actual field data.

The primary goal of the work we report here is to investigate the efficacy of using stochastic models to estimate Green's functions for use in an inversion for TDMTs. We perform a preliminary set of synthetic tests were we construct synthetic data for a pre-defined seismic source where the velocity model has stochastic variations. We then invert this data for various cases where the Green's functions are estimated for statistically identical, but deterministically different, velocity models. The second major goal presented here is to invert an field data set for the TDMT. The data were collected as part of a well perforation operation. To invert the data, we created Green's functions using velocity models that were smooth as well as those containing various degrees of stochastic variability in velocity and density. However, in all cases we were unable to obtain an acceptable agreement between the observed data and model. We speculate that the poor results of our inversion of actual field data is hampered by a poor estimate of the geologic model at the field site, as well as noisy data.

# Chapter 2

# Methods

## 2.1 The forward model

Seismograms in the far field can be modeled as a general Green's function integral representation solution to the elastic wave equation. This approach includes body force terms, boundary value terms, and initial value terms. The boundary and initial value terms can be expressed as equivalent body forces. Specifically, we can write the solution as

$$u_k(\mathbf{x}',t') = \int_{-\infty}^{\infty}\int_{V_0} G_{ki}(\mathbf{x}',t';\mathbf{x},t) f_i(\mathbf{x},t) dx^3 dt \tag{2.1}$$

where $u_k$ is the displacement seismogram, $G_{ki}$ is the Greens function describing the impulse response from source $i$ located at $\mathbf{x}$ to receiver $k$ at $\mathbf{x}'$, $f_i$ is the sum of the real and equivalent body forces, and $V_0$ is the source volume which contains the non-zero portion of $f_i$.

In the so-called far field, defined as several tens of wavelengths from the source, it's been shown that the equation 2.1 is essentially linear:

$$u_k(\mathbf{x}',t') = G_{ki,j}(\mathbf{x}',t';\mathbf{0},0) \otimes M_{ij}(\mathbf{0}). \tag{2.2}$$

where we've placed the origin at the seismic source, and the symbol $\otimes$ denotes time-domain convolution. $M_{ij}(\mathbf{0})$ is a rank-2 tensor describing the nine (or six independent) force couples that describe the seismic moment:

$$M_{ij} = M_{xy} = \begin{bmatrix} M_{xx} & M_{xy} & M_{xz} \\ M_{yx} & M_{yy} & M_{yz} \\ M_{zx} & M_{zy} & M_{zz} \end{bmatrix}. \tag{2.3}$$

The entity $M_{ij}$ describes the six possible independent moment couples, and has units of force times distance (e.g. $Nm$, or $J$). In many analysis of seismic data, the goal of the analysis is to resolve the terms of $M_{ij}$ under the assumption of a "point source" (e.g. focal-mechanism inversions commonly seen in earthquake analysis, such as Dahlen and Tromp, 1998, or Stein and Wysession, 2003). That is, the inversion assumes that the individual terms in $M_{ij}$ are scalars that share time dependance through a source-wavelet. The source wavelet, or the source time function, is identical for each moment term, but scaled by each term in $M_{ij}$. In this case, equation 2.2 becomes

$$u_k(\mathbf{x}',t') = G_{ki,j}(\mathbf{x}',t';\mathbf{0},0) \otimes [\hat{s}(t) M_{ij}(\mathbf{0})], \tag{2.4}$$

where $\hat{s}(t)$ is the source time function. However, for our work here, we relax the restriction of identical time dependance for all the terms in the moment tensor. Specifically, we treat the terms in $M_{ij}$ as time dependent, but with no requirement that they share the same time dependence:

$$u_k(\mathbf{x}',t') = G_{ki,j}(\mathbf{x}',t';\mathbf{0},0) \otimes [s_{ij}(\mathbf{0},t')M_{ij}] \tag{2.5}$$

where $s_{ij}(\mathbf{0},t')$ represents the source time function corresponding to each of the six independent force couples in the seismic moment tensor $M_{ij}$. The term $s_{ij}(\mathbf{0},t')M_{ij}$ can be combined into a single mathematical entity $m_{ij}(t) = s_{ij}(\mathbf{0},t')M_{ij}$, and is what our inversion scheme attempts to estimate.

## 2.2 Inversion method

The model presented in equation 2.5 can be rewritten as

$$u_k(\mathbf{x}',t') = G_{ki,j}(\mathbf{x}',t';\mathbf{0},0) \otimes m_{ij}(t) \tag{2.6}$$

and is interpreted as follows: the seismogram observed at location $\mathbf{x}'$ is the convolution of the Green's function with a TDMT describing the six independent force couples at the seismic source. We can Fourier transform equation 2.6 and thus perform the convolution as a multiplication in the frequency domain. Therefore we can re-write equation 2.6 as

$$\mathbf{u}_k = \sum_{i=1}^{P} G_{ij}(f)m_i(f) \tag{2.7}$$

where the observed data $\mathbf{u}_k$ is the sum of $i$ TDMT $m_i(f)$ multiplied with there respective Green's functions $G_{ij}(f)$. In matrix form,

$$\mathbf{u} = \mathbf{G}\mathbf{m}. \tag{2.8}$$

For $N$ frequencies, six independent TDMTs, and $K$ receiver stations, the matrices in equation 2.8 become

$$\begin{bmatrix} u_1(f_1) \\ u_1(f_2) \\ \vdots \\ u_1(f_N) \\ \\ u_2(f_1) \\ u_2(f_2) \\ \vdots \\ u_2(f_N) \\ \\ \vdots \\ \vdots \\ \\ u_K(f_1) \\ u_K(f_2) \\ \vdots \\ u_K(f_N) \end{bmatrix}_{KN\times 1} = \begin{bmatrix} \mathbf{G}_{1,1} & \mathbf{G}_{2,1} & \dots & \mathbf{G}_{6,1} \\ \\ \mathbf{G}_{1,2} & \mathbf{G}_{2,2} & \dots & \mathbf{G}_{6,2} \\ \\ \mathbf{G}_{1,3} & \mathbf{G}_{2,3} & \dots & \mathbf{G}_{6,3} \\ \\ \vdots & \vdots & \ddots & \vdots \\ \\ \mathbf{G}_{1,K} & \mathbf{G}_{2,K} & \dots & \mathbf{G}_{6,K} \end{bmatrix}_{KN\times 6N} \begin{bmatrix} m_1(f_1) \\ m_1(f_2) \\ \vdots \\ m_1(f_N) \\ \\ m_2(f_1) \\ m_2(f_2) \\ \vdots \\ m_2(f_N) \\ \\ \vdots \\ \vdots \\ \\ m_6(f_1) \\ m_6(f_2) \\ \vdots \\ m_6(f_N) \end{bmatrix}_{6N\times 1} \tag{2.9}$$

where, for example,

$$\mathbf{G}_{2,3} = \begin{bmatrix} G_{2,3}(f_1) & \dots & 0 \\ \\ \vdots & \searrow & \vdots \\ \\ 0 & \dots & G_{2,3}(f_N) \end{bmatrix}_{N\times N} \tag{2.10}$$

is the Green's function for the third receiver station and the TDMT term. To be clear, even though we refer to them as time domain moment tensors, it is the frequency domain versions of the TDMT that enter into equations 2.9.

This formulation is agnostic to the ordering of the terms as well as the number of data components: the ordering of the Green's functions $\mathbf{G}$ is dictated by the ordering of the data, which in turn dictates the ordering of the TDMTs $\mathbf{m}$. The number of data components is arbitrary as well. For example, each seismic station could have three component data, yielding $K$ seismograms, where $K$ would be three times the number of recording stations (each station recording three components of data).

This formulation also allows for simplifications in the assumed seismic source type. For example, if the source type consists of an explosion, then off-diagonal terms in the moment tensor, $m_{i\neq j}(t)$ can be assumed to be zero with only the three on-diagonal terms in $m_{ij}(t)$ remaining. In this case, there would only be three TDMTs in equation 2.9, which would reduce the dimensionality: $\mathbf{G}$ reduces to $KN \times 3N$ and $\mathbf{m}$ reduces to $3N \times 1$. If it's further assumed that the explosion is

purely isotropic, then the diagonal terms in the TDMT are all equal, allowing the further reduction in dimensions: $\mathbf{G}$ would reduce to a $KN \times N$ and $\mathbf{m}$ becomes $N \times 1$. Note however, that $\mathbf{u}$ always remains a $KN \times 1$ vector.

The system of equations shown in 2.9 can be solved using generalized least squares:

$$\mathbf{m} = \left(\mathbf{G}^{\dagger}\mathbf{W}_d^{\dagger}\mathbf{W}_d\mathbf{G} + \theta^2\mathbf{W}_s^{\dagger}\mathbf{W}_s\right)^{-1} \times \mathbf{G}^{\dagger}\mathbf{W}_d^{\dagger}\mathbf{W}_d\mathbf{u} \tag{2.11}$$

where $\mathbf{W}_d$ is a data weighting matrix, $\mathbf{W}_s$ is the model weighting matrix, and $[\cdot]^{\dagger}$ denotes the Hermitian transpose. Note that the solution given by 2.11 is in the frequency domain; the vector $\mathbf{m}$ contains the spectra of the estimated TDMTs which can, if desired, be converted to the time domain via the inverse Fourier transform.

### 2.2.1 Green Function Estimation

Any inversion problem is attempting to fit the observed data to data predicted by the geophysical model. In our case, the geophysical model is given by equation 2.6, which states that the data is a convolution of the TDMTs and the Green's functions. The matrix $\mathbf{G}$ is commonly referred to as a predictor matrix, because when multiplied with the model parameters $\mathbf{m}$ will predict the data. The goal is to find a set of model parameters, in this case the TDMTs, that minimize the $L2$ norm misfit between the predicted and observed data.

The elements in $\mathbf{G}$ are the frequency domain Green's functions that describe the impulse response of the Earth from the (assumed) point source and the receiver station. Mathematically, this is akin to convolving a Dirac delta function with the Earth. To estimate Green's functions, we need to have knowledge of the Earth structure as well as the type of seismic source. In the event that we have an accurate model of the Earth, we must also make assumptions about the type of seismic source. Specifically, we must assume which elements of the moment tensor are populated. To compute the Green's functions, we use a special case of equation 2.5;

$$G_{ki,j}(\mathbf{x}',t') = I_k(\mathbf{x}';\mathbf{x}) \otimes \widehat{m}_{ij} \tag{2.12}$$

where $I_k$ is the Earth's impulse response from the source location $\mathbf{x}$ to receiver $k$ located at $\mathbf{x}'$, $\widehat{m}_{ij}$ is the $3 \times 3$ impulse force moment tensor. Note the tensor $\widehat{m}_{ij}$ contains no time dependance, as the terms are all scalar values whose purpose is to scale $I_k$. In other words, the terms in $\hat{m}_{ij}$ are scaled Dirac delta functions.

At this point, the distinction between "Green's function" and the "Earth's impulse response" must be made. Mathematically, they are identical. However from a numerical standpoint they are different. To estimate the Green's functions we must solve equation 2.12 numerically, in our case using a Sandia-developed program called Paralastic. This program uses a staggered-grid finite difference approximation to solve the elastic wave equation for time domain displacements. A true Dirac delta function is numerically unstable in a finite difference scheme, so the terms in $\hat{m}_{ij}$ must become a band-limited (hence finite-length in time) functions that are then convolved with

the predefined Earth model, given by $I_k(\mathbf{x}';\mathbf{x})$. The convolution is accomplished by numerically solving the elastic wave equation where $I_k(\mathbf{x}';\mathbf{x})$ is the Earth model describing seismic velocities and densities at all points in the model and the moment tensor $\hat{m}_{ij}$ is approximated by $a(t)\hat{m}_{ij}$. In this context, $a(t)$ is a band-limited function that, when multiplied by $m_{ij}$, approximates the scaled Dirac delta functions in $\hat{m}_{ij}$. In essence, $a(t)\hat{m}_{ij} = m_{ij}(t)$. The bandwidth of $a(t)$ is controlled by the seismic velocities in the Earth model as well as the physical size of the discrete nodes in the density/velocity model.

Let us consider the following examples.

1. An isotropic explosion source with unit amplitude: In this case, the off-diagonal terms in $\hat{m}_{ij}$ are zero and the diagonal terms are all unity.

$$G_{ki,j}(\mathbf{x}',t') = I_k(\mathbf{x}';\mathbf{x}) \otimes a(t) \begin{bmatrix} 1 & 0 & 0 \\ 0 & 1 & 0 \\ 0 & 0 & 1 \end{bmatrix} \tag{2.13}$$

   Because the diagonal terms are all the same, $a(t)\hat{m}_{ij}$ collapses to a vector and 2.15 becomes

$$G_{ki,j}(\mathbf{x}',t') = I_k(\mathbf{x}';\mathbf{x}) \otimes a(t). \tag{2.14}$$

2. A non-isotropic explosion. Consider the case where a directed explosion, for example one designed for well perforation, is designed such that the horizontal component explosive energy is much greater than the vertical component energy. Let us further consider the case where the horizontal component energy, though similar, are not exactly the same. For example let's assume that the ratio between the x, y, and z direction of energy is 1:0.9:0.2. In this case, equation 2.12 becomes

$$G_{ki,j}(\mathbf{x}',t') = I_k(\mathbf{x}';\mathbf{x}) \otimes E_{tot}a(t) \begin{bmatrix} 1.0 & 0 & 0 \\ 0 & 0.9 & 0 \\ 0 & 0 & 0.2 \end{bmatrix} \tag{2.15}$$

   where $E_{tot}$ is related to the total explosive yield.

## 2.3 Stochastic Earth models

From a seismic perspective, it's convenient to model the Earth as a collection of deterministic layers or bodies, each with assigned material properties such as seismic velocity and density. Although this first-order approximation can be useful, it's well known that most portions of the Earth's crust are highly heterogeneous, even within a given layer. In such a case, one can describe the heterogeneities statistically using stochastic models. For example, it's been demonstrated that the crystalline portion of the Earth's crust can be approximated using stochastic density and velocity distributions with self-affine fabrics (e.g. Holliger and Levander, 1992; Holliger *et al.*, 1994). The success of this stochastic approach to characterizing the crust is evidenced by the similarity of

synthetic seismograms to recorded field data (Holliger and Levander, 1994; Holliger *et al.*, 1994; Levander *et al.*, 1994a,b; Hurich 1996; Hurich and Kocurko, 1999) as well as successful wave form inversion schemes (Poppeliers and Levander, 2004; Poppeliers, 2007; Poppeliers, 2009). The justification of using stochastic models to simulate the Earth's crust is that in most cases the impedance structure is so complex, that it's only tractable to represent a impedance as an equivalent statistical model. Although the above referenced works focused on the Earth's crystalline crust, such methods can also be used to model unconsolidated materials.

A recipe for creating a discrete 3D stochastic field can be described as follows (Goff *et al.*, 1994):

1. Define a 3D power spectrum as a discrete signal
2. Take the square root of this signal
3. Give the signal a uniformly random phase $\phi$, forming the complex-valued spectrum
4. Perform an inverse Fourier transform to obtain the field

Because of the uniformly random phase $\phi$, the resulting field has velocities which obey a normal distribution. The structure and autocorrelation of the field is according the power spectrum used. For the work here, we use a von Karman power spectrum, as it appears to most closely represent the power spectrum of mapped Earth heterogeneities.

The analytic radial von Karman power spectrum is given by

$$P(k) = \frac{4\pi\nu a_x a_y a_z}{(1+k^2)^{\nu+1}} \tag{2.16}$$

which corresponds to a radial autocorrelation function in the space domain (Goff and Jordan, 1988):

$$C(r) = \frac{G_\nu(r)}{G_\nu(0)}, \tag{2.17}$$

where

$$G_\nu(r) = r^\nu K_\nu(r), \tag{2.18}$$

$K_\nu(r)$ is the second modified Bessel function of fractal order $\nu$, $\Gamma$ is the Gamma function and $\nu$ is the Hurst exponent. Additional terms are defined as

- $a_x$, $a_y$, $a_z$ are the correlation lengths in the $x$, $y$ ,and $z$ directions, respectively
- $k$ is the weighted radial wavenumber, $\sqrt{k_x^2+k_y^2+k_z^2}$, where

  $k_x = 2\pi/\lambda_x$,
  $k_y = 2\pi/\lambda_y$,
  $k_z = 2\pi/\lambda_z$,

and $\lambda$ is wavelength

- $x$, $y$, and $z$ are the autocorrelation lags in their respective directions as well as the $x$, $y$, and $z$ coordinates of the stochastic field
- $r$ is the weighted radial autocorrelation lag, $\sqrt{x^2/a_x^2 + y^2/a_y^2 + z^2/a_z^2}$
- $\nu$ is the Hurst exponent, which is related to the fractal dimension $D = E + 1 - \nu$ where $E$ is the Euclidian dimension ($E = 3$ for three-dimensional models).

To parameterize a stochastic field, we first define the the wavenumber cutoff in the $x$, $y$, and $z$ directions, which in turn controls the correlation lengths of the field in the respective directions. For the work here, we set the correlation lengths to be $a_x = a_y = 200m$ and $a_z = 100m$, and fix the Hurst exponent to $\nu = 0.8$. The corner wavenumber cutoff $k_{x,y,z} \propto 1/a_{x,y,z}$ controls the correlation length of the von Karman field. Above the corner wavenumber, the power spectrum exhibits power-law decay, which governs power-law (fractal) scaling of structure in the spatial domain. Below the corner frequency, the power spectrum is white.

To generate a stochastic velocity model, we first define a background velocity model $V_0(x,y,z)$ which represents the gross, deterministic structure of the Earth as determined by, for example, seismic tomography. We then generate a stochastic field and scale it to the root-mean-square magnitude of the background velocity, $\delta V(x,y,z)$. Note that in general,

$$\frac{\delta V(x,y,z)}{V_0(x,y,z)} << 1. \tag{2.19}$$

The stochastic velocity model is then constructed as

$$V(x,y,z) = V_0(x,y,z) + \delta V(x,y,z). \tag{2.20}$$

Note that this method can proceed for $V_p$, $V_s$, and/or density separately, or for just one of these parameters, where the others scale appropriately (Figure 2.1).

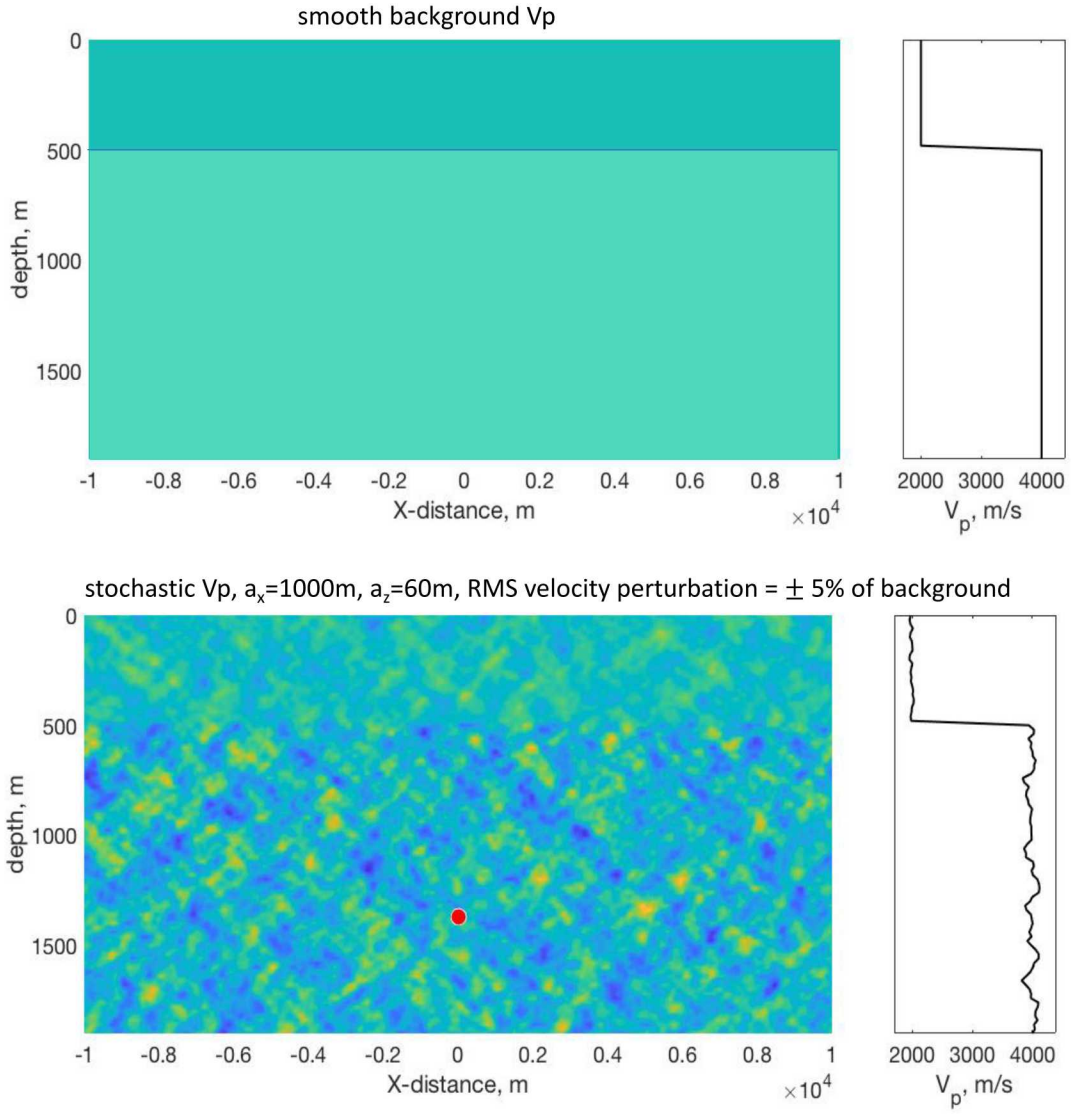


**Figure 2.1.** An example of a 2D stochastic $V_p$ model. In this example, the model has two gross layers. The top panel shows the background Vp, with no stochastic variability. The bottom panel shows an example of applying a stochastic variation to the background velocity. The stochastic variability in $V_p$ is parameterized by a $\pm 5\%$ RMS variation about the background velocity, with the correlation lengths $a_x = 1000m$, and $a_z = 60m$

# Chapter 3

# Results

In this chapter, we show the results of several synthetic tests as well as the results from inverting actual field data. The synthetic tests are designed to explore the effects of stochastic variability on the inversion results as well as demonstrate our inversion's ability to extract multiple terms of the source time function tensor.

## 3.1 Synthetic tests

The synthetic tests involve constructing an Earth model with and without stochastic variability in the density/velocity properties, computing synthetic three-component data, and the corresponding Green's functions. All of the forward modeling (as well at the Green's function calculations) are performed using the Sandia-developed Paralastic code. For the synthetic tests, we use an Earth model that is designed to approximately mimic an actual field site, located outside of Winnemucca, NV (Figure 3.1). This site is the location of an active geothermal well field, and contains significant topography and geologic variability. Although we retain the topographic features in the synthetic tests, we simplify the gross density/velocity structure to a three-layer half space. The bottom two layers simulate typical Earth materials ($V_p > V_s$, $\rho >> 1$ kg/m$^3$) whereas the top layer is modeled as air ($V_p = 0.35$ km/s, $V_s = 0, \rho = 1.225$ kg/m$^3$). The synthetic, three-component receiver stations are placed at the same position as the those used during the actual field experiment, as is the synthetic source.

### 3.1.1 Benchmark tests: no stochastic variation

#### Isotropic explosion

The first simulations are designed to verify that the inversion can estimate TDMTs in the simplest case. Figure 3.3 shows the results of inverting synthetic data where there was no stochastic perturbations on the background velocity field, and the (single) source is explicitly isotropic. For this simulation, we computed the Green's functions by inserting a sourcing wavelet at the location indicated in Figure , where the source wavelet was a Dirac delta, filtered to a passband of $19-200$Hz with equal amplitude in the $x$, $y$, and $z$ directions. The data were constructed similarly, but the

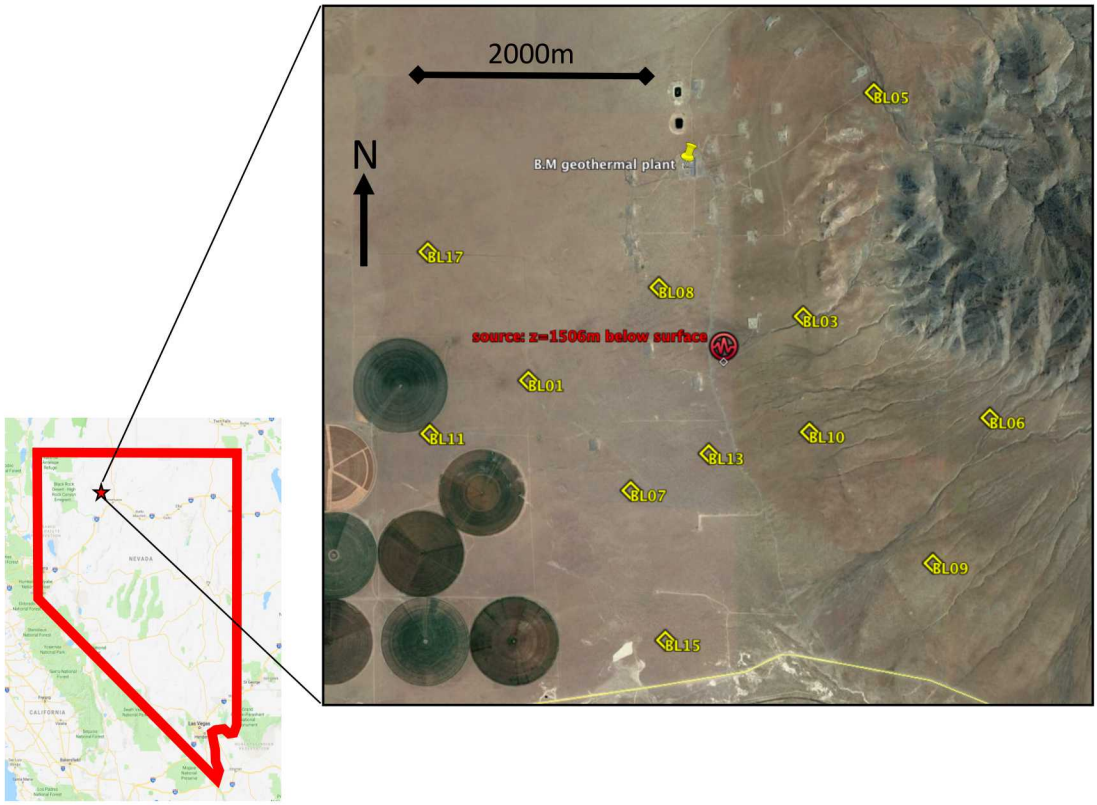


**Figure 3.1.** The field site, located outside of Winnemucca. All the synthetic tests use the geometry of the actual site, including the topography and the receiver locations.

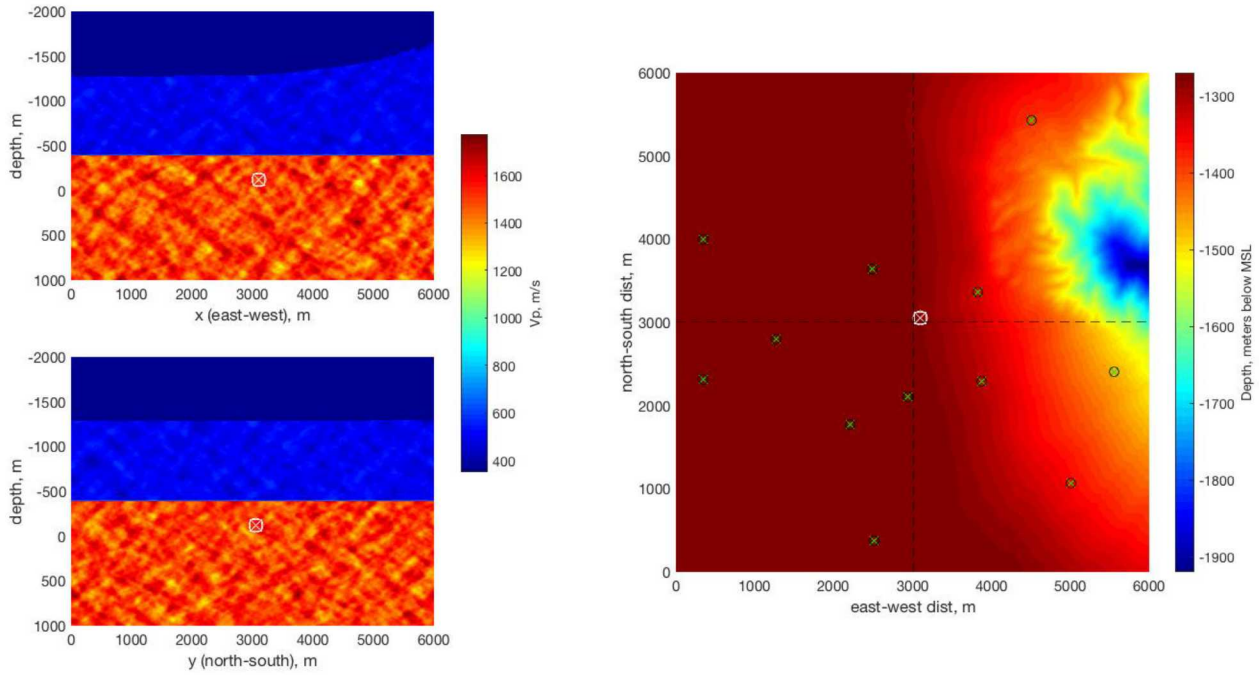


**Figure 3.2.** An example of a 2D stochastic $V_p$ model, where the model geometry and topography mimic those of the actual field site (Figure 3.1). In this example, the model has three layers: two Earth layers an an air layer. The two panels on the left show 2D slices though the 3D model, where the stochastic variability in $V_p$ is parameterized by a $\pm 5\%$ RMS variation about the background velocity, with the correlation lengths $a_x = a_y = 200m, a_z = 100m$. The source locations are shown as the white, encircled $X$. The panel on the right shows the topography and the geometry of the recording array (green $x$'s, circled in black). The two dashed lines show the locations of the 2D slices in the left hand panels, and the white, encircled $X$ indicates the location of the seismic source, projected to the surface. Note that the depth is indicated as meters below mean sea level, with positive being downwards.

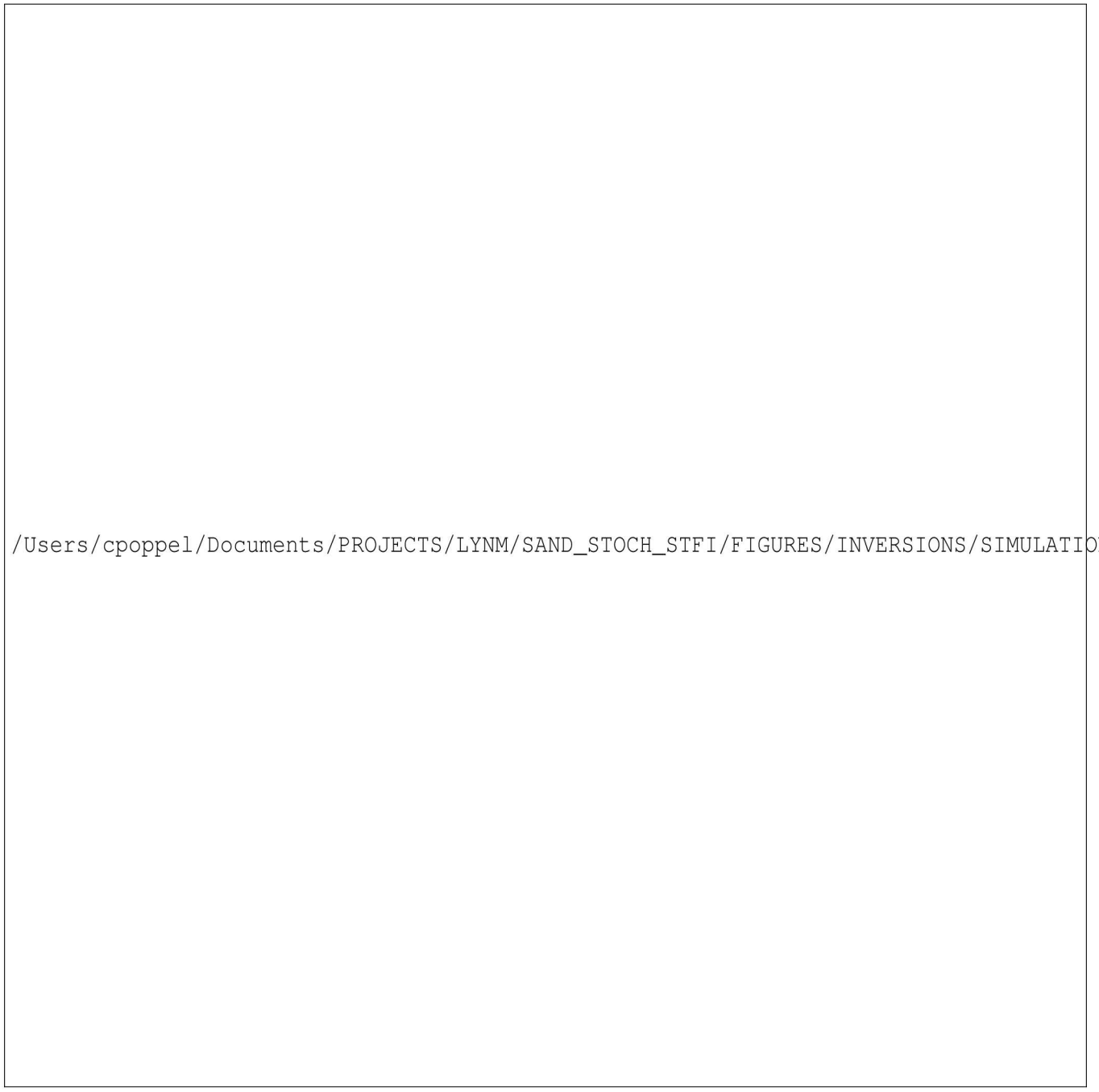


**Figure 3.3.** Inversion results for a simulated isotropic source, and isotropic Green's functions. This represents the simplest test case and serves to verify that the concept is sound. The top panel shows the estimated source time function (with units of Newton $\times$ meters, or Nm) and the bottom panel shows the results of convolving the estimated TDMT with the Green's functions, which we term 'computed data', and is shown in red. Note that the observed data is also plotted (in black) but is not visible as it's virtually identical to the computed data. The traces are arranged by component and station: e.g. each group of three traces represent the east, north, and vertical components

sourcing wavelet was a 10Hz Ricker wavelet with equal amplitude in the $x$, $y$, and $z$ directions. Figure 3.3 shows both the estimated TDMT as well as the the convolution of the Green's functions with the TDMT (termed the computed data). Note that in this case the computed data is virtually identical to the observed (synthetic) data.

**Non-isotropic explosion**

The TDMT of a cylindrical explosion may be represented as follows:

$$m_{ij}(t) = A(t) \begin{pmatrix} 1 & 0 & 0 \\ 0 & 1 & 0 \\ 0 & 0 & g \end{pmatrix} \qquad (0 < g \leq 1)$$

where $A(t)$ is a finite-time source time function that's scaled by the terms in the moment tensor. The physical interpretation of this type of mechanism is that most of the explosive energy is directed in the (radially symmetric) horizontal directions, with less energy being directed in the vertical direction. However, note that in this representation, the source time function is identical in all three components, but just scaled differently. This type of moment would be expected, for example, in a well-perforation operation where the well bore is vertical. To simulate this, we explicitly assign the relative amplitude of the diagonal terms in $\hat{m}_{ij}$ to be $|m_{xx}| = |m_{yy}| = 1/4|m_{zz}|$, where the sourcing wavelet is identical for all three terms in $\hat{m}_{i=j}$. The notation $|\cdot|$ indicates the maximum amplitude over the finite time space of the sourcing wavelet. The three TDMTs estimated from inverting the synthetic data all show the appropriate relative scaling, and when convolved with the Green's functions, match the observed data (Figure 3.4).

**Non-isotropic explosion with off-diagonal elements**

The moment tensor for this test was defined as

$$m(t)_{ij} = A_{ij}(t) \begin{pmatrix} 1 & 0.3 & 0.2 \\ 0.3 & 1 & 0.1 \\ 0.2 & 0.1 & 1 \end{pmatrix}$$

where $A_{ij}(t)$ is an arbitrary function for each $ij$ element of the moment tensor. In other words, the moment tensor here is fully time dependent (and as such, termed the time domain moment tensor) where each of the six independent elements can be unique in terms of amplitude and waveform. This represents the most general case of a time domain moment tensor.

Figure 3.5 shows the results of inverting the synthetic data. The data were constructed using the velocity model shown in figure 3.2, but with no stochastic variation. The inversion estimated the six independent time domain moment tensor terms at the correct relative amplitudes, but there is an imperfect reconstruction of the data. In other words, when we convolved the estimated time domain moment tensor with the model Green's functions, the resulting computed data did not perfectly match the observed data. We attribute this to 1) the fact that we band-limited the inversion

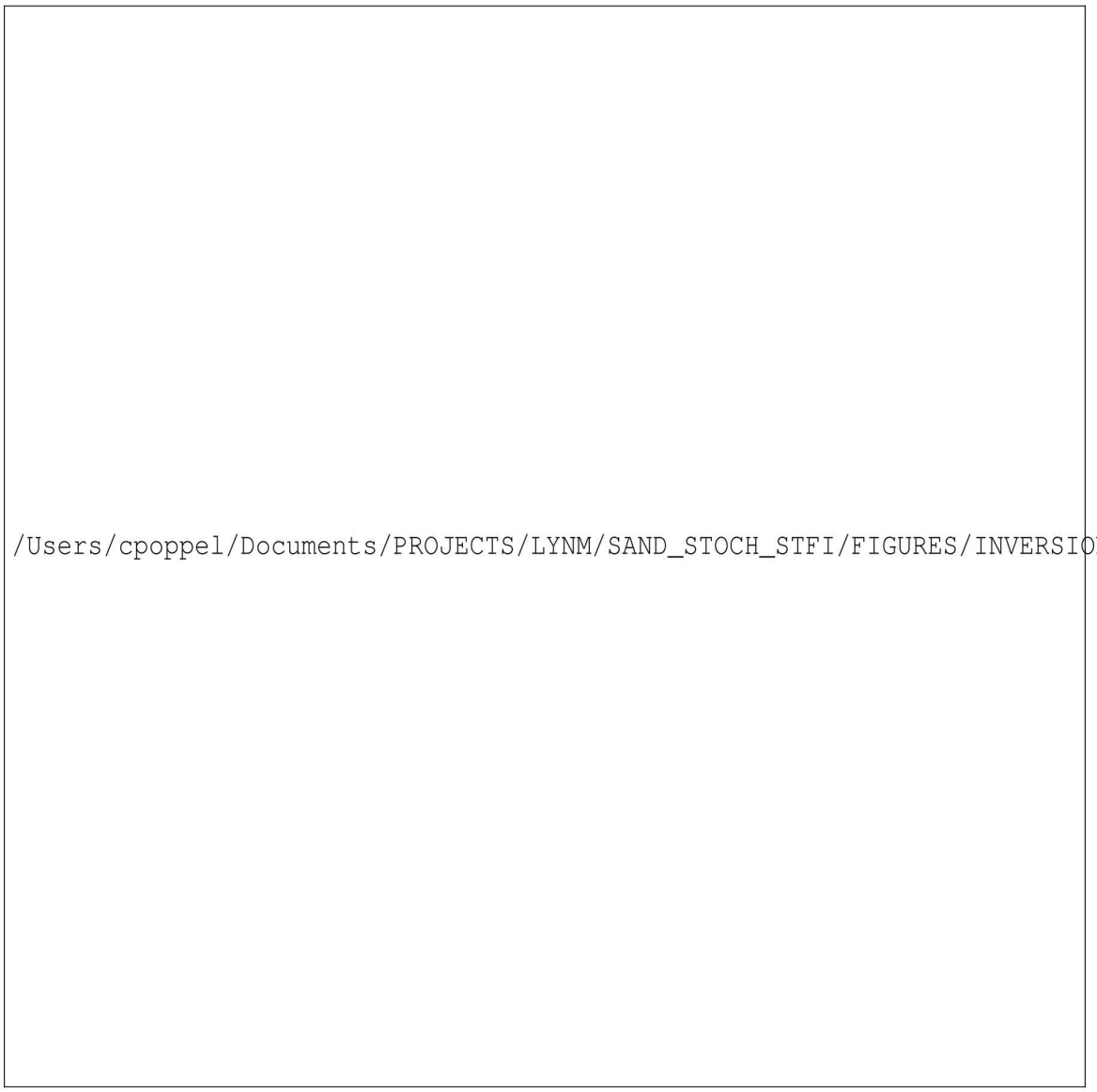


**Figure 3.4.** Same as Figure 3.3, but the relative amplitude of the TDMT terms were explicitly set to $|m_{xx}| = |m_{yy}| = 1$, and $|m_{zz}| = 0.25$. The three estimated TDMTs are shown in the top panel. Note that the estimated TDMTs corresponding to $m_{xx}(t)$ and $m_{yy}(t)$ are virtually identical, causing them to plot atop one another. Note also that the maximum amplitude of the $m_{zz}(t)$ is roughly one-quarter that of the other two, which is the expected result.

to a 1-40Hz passband in order to avoid low frequency instabilities in the matrix inversions and 2) we decimated the data by a factor of 10 to speed up the computations. However, the computed data matches the observed data quite well for the first 1-2 seconds. It's not until t>2 seconds that the misfit becomes more pronounced. Regardless, based on the results of this simulation, we are confident that the inversion scheme performs as expected.

### 3.1.2 Benchmark tests, 2.5% RMS stochastic variation

In this section, we perform similar tests as before, but insert stochastic density and velocity perturbations in into the velocity model. The goal is to explore how stochastic variation, which is known to cause seismic scattering, effects the result of our inversion. Specifically, the inverse method that we outline in the previous chapter relies on an accurate estimation of the Green's function for a given term in the moment tensor. However, the Earth's density/velocity structure can never be perfectly known. Density/velocity models of the Earth derived from, for example, seismic tomography produce smooth models. If these models are used to estimate Green's functions, the resulting Green's functions will not account for the (potential) multiple scattering produced by small-scale heterogeneities. We can simulate, in a statistical sense, the background heterogeneities but how the effects of them propagate into the inverse solutions for the TDMTs are not clear. We will briefly explore this question in this section.

For the simulations in this section we construct synthetic data for two cases: a isotropic (explosion) source and a non-istropic source. However, for these tests we construct two stochastic velocity models, each with identical background velocity and stochastic parameters (correlation length and fractal dimension). The only difference in the models is that the seed value for the random number generator (used to generate the random phase in the frequency-domain stochastic field) was different for each model. Thus, even though the two models have identical statistical, or stochastic, parameters, the individual realizations of the stochastic velocity models is different. The goal of these simulation is to determine the sensitivity of the inversion results to differences in stochastic realizations in both the time and frequency domain.

#### Isotropic explosion

This simulation assumes a pure explosion source ($m_{xx}(t) = m_{yy}(t) = m_{zz}(t)$). We constructed two synthetic data sets, one for each realization of the stochastic background. As expected, when the data and the Green's functions are constructed using the same velocity model, the inversion is able to exactly recover an STF, that when convolved with the Green's function, perfectly match the observed data (Figure 3.6, top panel). However, when the data are constructed from a model that is different from that used to construct the Green's function, the computed data doesn't match the observed data as well (Figure 3.6, bottom panel).

For further discussion, we define the recovered TDMTs as follows: the "blue TDMT" is that which is estimated by inverting the data where the same stochastic realization of the velocity is

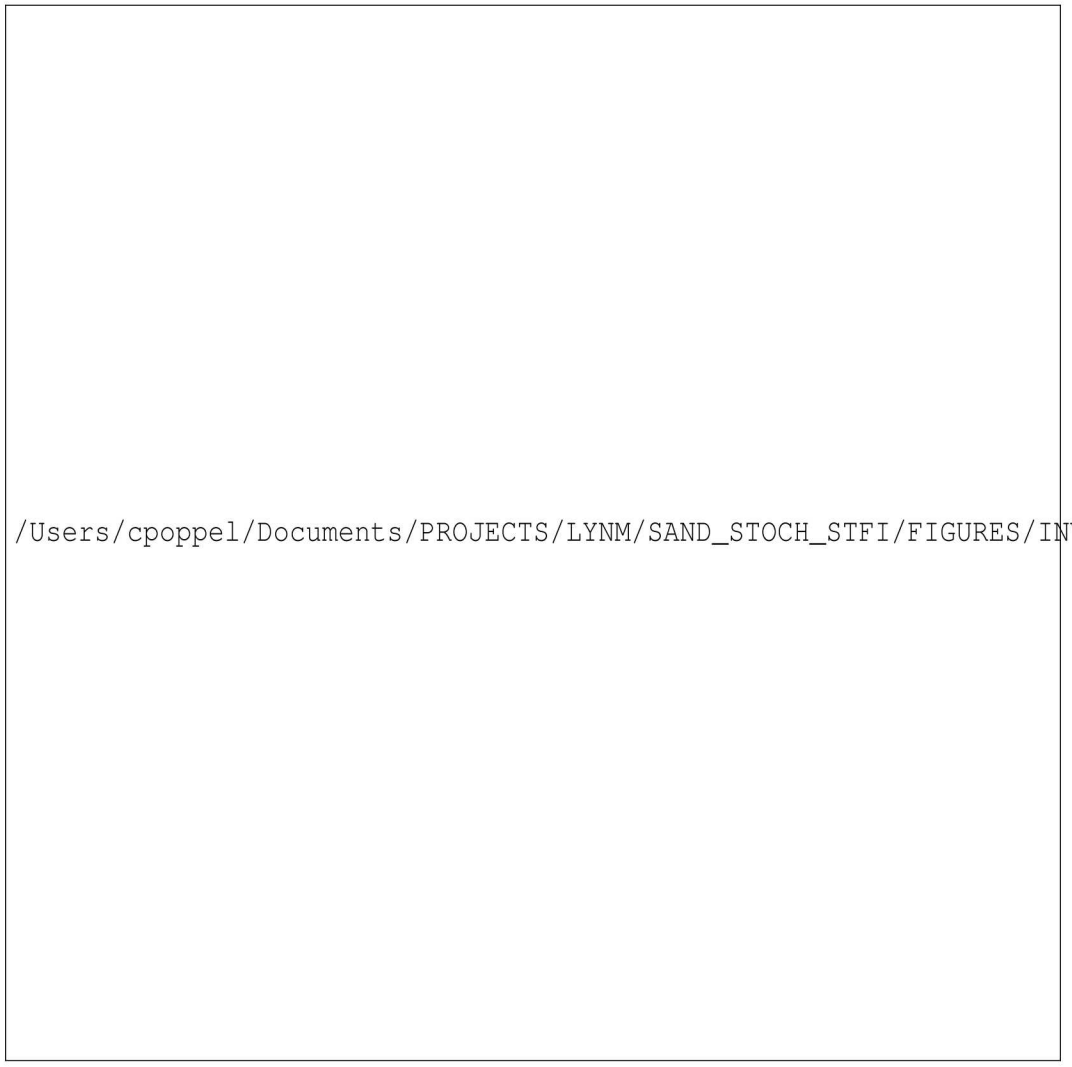


**Figure 3.5.** Results for inverting synthetic data for six independent TDMTs. The top panel shows the estimated TDMTs, arranged to correspond to the terms on the actual tensor. Note that the relative amplitudes of the estimated TDMTs match that of the input model. The bottom panel shows the observed (in this case, synthetic) data (black) overlain by the computed data (red). Note that the reconstruction isn't perfect, which we attribute to the numerical effects of data and Green's function decimation.

used to create both the synthetic data and the Green's functions. The "red TDMT" is the TDMT estimated where a different stochastic realization of the velocity model is used to estimate the Green's functions.

For the TDMTs, the maximum amplitude of the red TDMT is only half that of the blue TDMT, and the is energy is spread later in time for the red TDMT. Also, the red TDMT shows small, but significant, high frequency oscillation near $t = 0$. The blue TDMT is considerably better behaved, in that it closely resembles the Ricker sourcing wavelet. Also, the amplitude and duration of the high frequency oscillations near $t = 0$ are significantly smaller than those seen in the red TDMT, but they are still apparent. When examining the correspond power spectra of the TDMTs, the blue TDMT contains more energy for $f < 22$Hz, than the red TDMT. For $f > 22$Hz, the energy content appears relatively similar. Also, for $f < 22$Hz, the power spectrum of the red TDMT displays significantly more variance than blue TDMT power spectrum. It is not clear why this is the case.

#### Non-isotropic explosion

The simulations here are similar to those in section 3.1.2: We assume a cylindrical explosion where the moment tensor terms are scaled as $|m_{xx}| = |m_{yy}| = 1/4|m_{zz}|$. Also, similar to the test performed in the previous sub-section, we compute two stochastic realizations of the velocity model. Let us define two cases: Case 1 is when the identical stochastic model is used to generate the synthetic data as well as the Green's functions. Case 2 is when the stochastic model used to generate the data is different than that used to estimate the Green's function. To be clear, however, the stochastic parameters (e.g. fractal dimension, correlation length, etc.) are identical; the only difference is the seed used to generate the random phase.

For Case 1, the estimated TDMT, that when convolved with the Green's functions, produce computed data that almost perfectly matches the observed data (Figure 3.8, top panel). The relative maximum amplitude of the estimated STFs are at the correct relative amplitude. However, for Case 2, the computed data does not match the observed data as well (Figure 3.8, bottom panel). We observe that the maximum amplitude of the estimated STFs for Case 2 are also approximately half of those for Case 1, and that the estimated STFs for Case 2 are "ringier". When we compare the power spectra of the estimated STFs, the spectra for Case 1 are smoother than those for Case 2, and that the Case 2 STFs contain significantly less energy in the higher frequency (f¿25Hz) portion of the spectrum.

### 3.1.3 Cylindrical explosion with off-diagonal terms

For the final test, we simulate a non-isotropic explosion where the relative amplitude of the terms in the time dependent moment tensor are

$$m_{ij}(t) = A(t) \begin{pmatrix} 1 & 0.1 & 0.2 \\ 0.1 & 1 & 0.3 \\ 0.2 & 0.3 & 0.7 \end{pmatrix}. \tag{3.1}$$


**Figure 3.6.** Inversion results for two different stochastic realizations. In the top panel, the stochastic velocity model used to generate the synthetic data is identical to that used to estimated the Green's functions. Note the virtually perfect match between the observed data and data computed by convolving the estimated TDMT with the Green's functions. In the bottom panel, the stochastic model used to estimate the Green's function was different than that used to generate the synthetic data. In this case, the observed data is significantly different than the data computed by convolving the estimated TDMT with the Green's functions used in the inversion. Note that only the data from four stations is being shown for clarity.

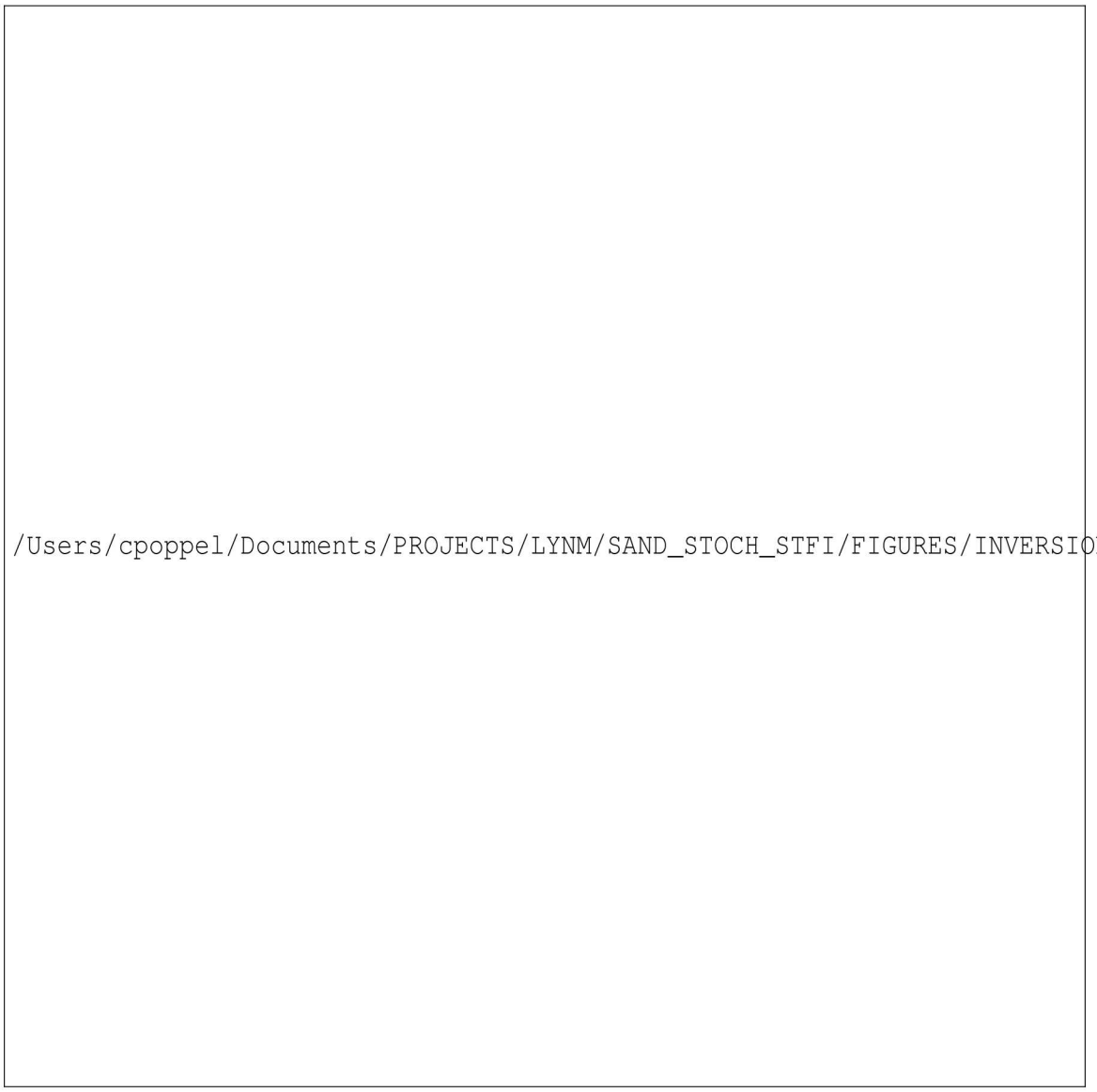


**Figure 3.7.** The recovered TDMTs originally shown in Figure 3.6 as well as their corresponding power spectra. The blue lines correspond to the case where the realization of the stochastic velocity model is identical for both the Green's function computation and the generation of the synthetic data (top panel of figure 3.6). The red lines correspond to the case where the stochastic realizations used to generate the Green's function and the data were different (bottom panel of figure 3.6). In this case, the stochastic parameters and the background model were identical; the only difference was the actual stochastic realization.


**Figure 3.8.** The top panel shows the inversion results when the same realization of the stochastic velocity model is used to generate both the synthetic data and the Green's functions. The bottom panel shows the results when we invert the same data, but use a different realization of the stochastic velocity model to estimate the Green's functions.

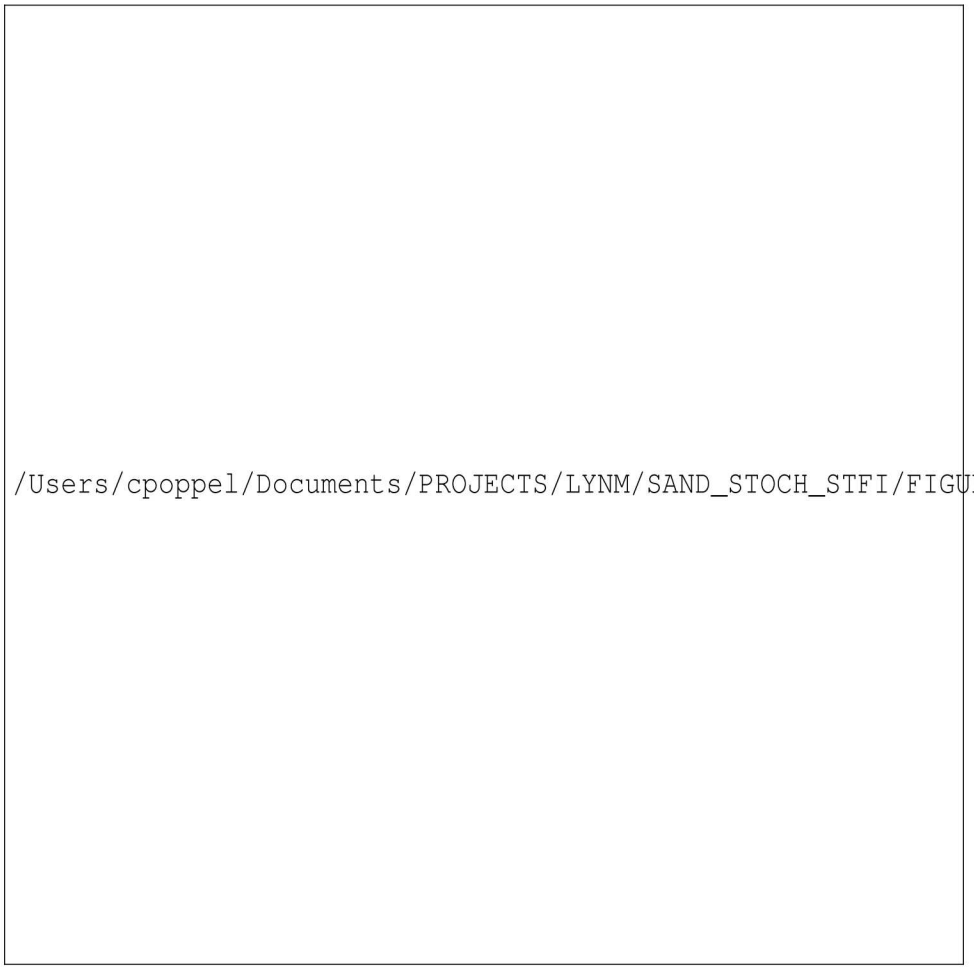


**Figure 3.9.** The recovered TDMTs originally shown in Figure 3.8 as well as their corresponding power spectra. The blue lines correspond to the case where the realization of the stochastic velocity model is identical for both the Green's function computation and the generation of the synthetic data (top panel of figure 3.8). The red lines correspond to the case where the stochastic realizations used to generate the Green's function and the data were different (bottom panel of figure 3.8). In this case, the stochastic parameters and the background model were identical; the only difference was the actual stochastic realization.

For this test, the individual Green's functions are computed using the smooth velocity model, whereas the data are simulated using a velocity model that has a stochastic variation of 1% of the background property. This test is designed to verify that our inverse scheme can resolve the six independent terms of the time dependent moment tensor, even in the case where the data result from a model that is not identically matched by the Green's function estimation. In other words, when inverting actual data, it's highly unlikely that the Green's function used in the inversion is a perfect reproduction of the Earth. There is a mismatch between the data and the Green's function that will degrade the results. The test performed here is attempting to mimic this situation. Regardless, the inversion is able to recover the six independent TDMTs at the correct relative amplitudes (Figure 3.1.3). However, when using these moment tensor terms to compute the data there is a slight, but significant, mismatch between the observed data and the computed data. This is attributed to the fact that the velocity model used to generate the synthetic data is different than that used to compute the Green's functions.

## 3.2 Blue Mountain

On December 15, 2017, a series of down-well explosions were conducted in the attempts to increase the permeability of a formation known to contain geothermal fluids (Figure 3.12). The well, located outside of Winnemucca, NV, is operated by AltaRock Energy, Inc., and was perforated with a series of five explosive charges. We collected data on twelve three-component seismic stations and recorded a total of five well perforation shots. For each seismic station, we deployed a single three-component Sercel L-28 geophone buried to a depth of approximately 0.5 meters. The data were logged to a RefTek RT 130 datalogger, sampling at 200Hz. Figure 3.12 shows data for the only that had a signal-to-noise ratio greater than unity. Note that for this shot, the charge consisted of approximately 14kg of HMX and Aluminum, approximately 1000m below the ground surface, and was detonated within the fluid-containing bedrock.

Because only one shot had a signal-to-noise ratio greater than unity, we made the decision to only invert this single dataset. The three component data was instrument corrected, de-meaned and filtered to a passband of 1-15Hz. Prior to inversion, we estimated the Green's functions using a 1-D geologic model based on the local topography and published tomographic results (Optim, 2007). However, the velocity models presented in this report were created by seismic refraction tomography along 2D profiles that only provided spatially sparse coverage, and only provided velocity information to a maximum depth of about 300-400m. This is primarily due to the fact that these models were created with the goal of mapping fault structures near the interface between the unconsolidated basin fill and the underlying bedrock. Furthermore, the strong velocity contrast between these two units is steeply dipping to the west. Although we are able to model the topography in our geologic model, at the time of this writing we have not modeled the dipping layers seen in the tomographic models.

We first performed the inversion where we constrained the solution to include only time dependent moment tensors that lie on the the diagonal: i.e. $m_{ij}(t)$, where $i = j$ (figure 3.13). We also inverted the data for all six independent TDMT terms. For this first inversion, we inverted

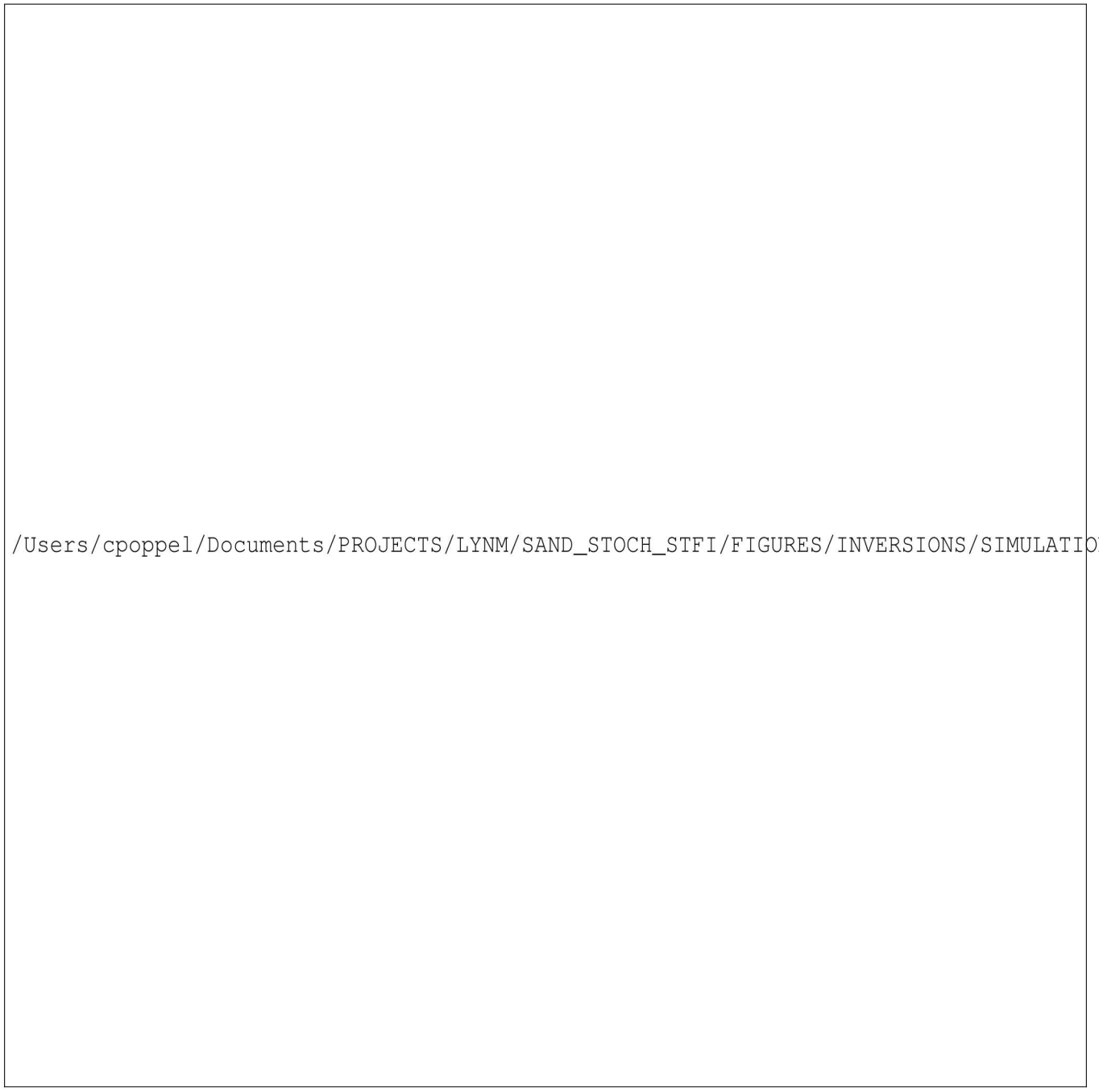


**Figure 3.10.** The recovered TDMT, where the data are simulated using the relative amplitudes shown in equation 3.1. Note that for this simulation, the Green's functions were computed using a smooth velocity model (no stochastic variation) whereas the data were simulated using the same background velocity model but with a stochastic variation. The stochastic variation is scaled to be 1% of the background model parameter. The inset shows the that the computed data doesn't perfectly match the observed data, which is attributed to the slight difference between the models used to simulate the data and the Green's functions. Regardless, the estimated time dependent moment tensors are of the correct amplitude.

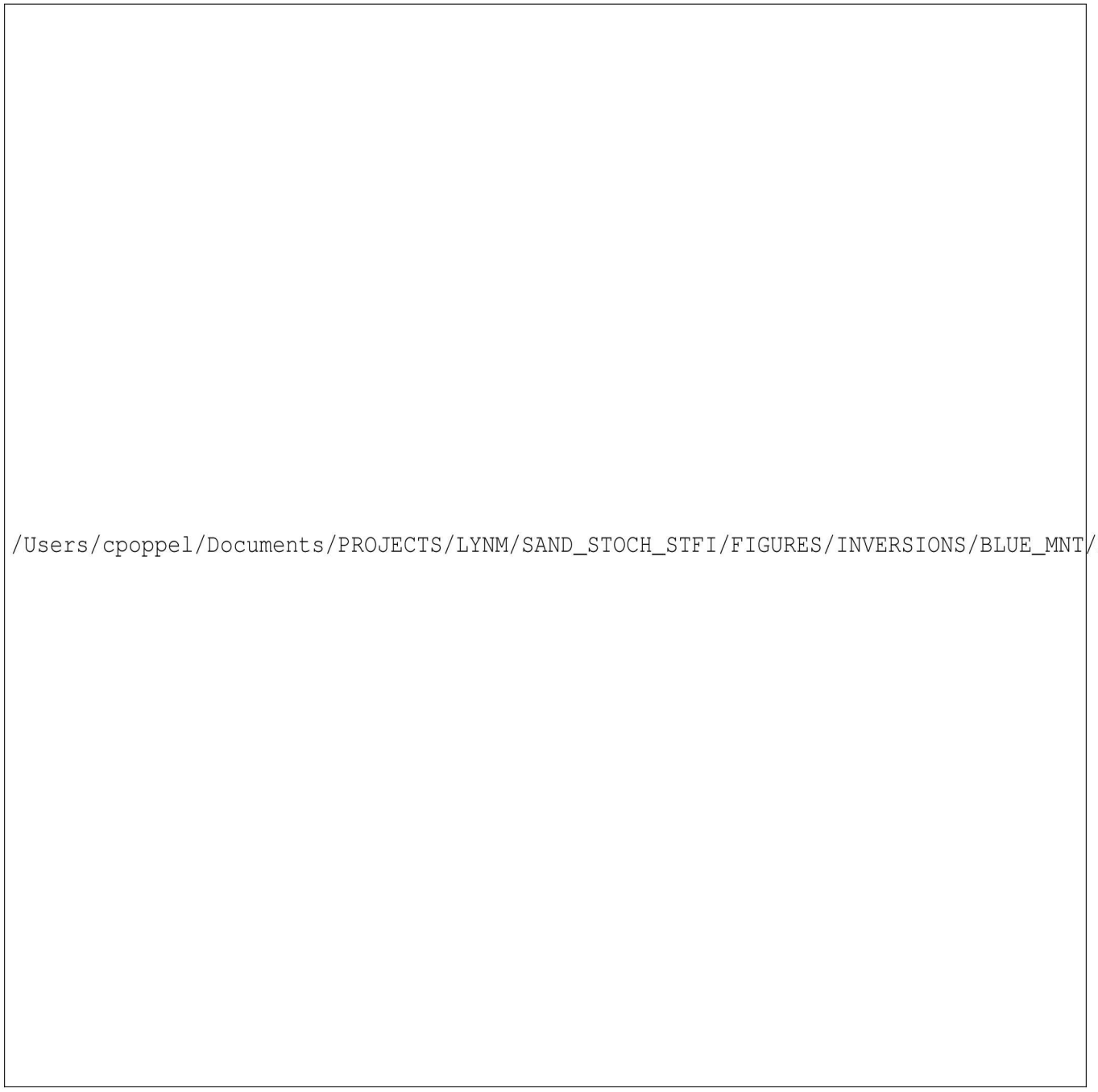


**Figure 3.11.** 1D velocity model for the Blue Mountain field site. The panels on the left are cross sections through the model, where the color corresponds to the velocity. The panel on the right shows the topography, where the topographic highs are indicated by the cool colors and the topographic lows are indicated by the warm colors. The white, encircled 'x' indicates the location of the explosive source. Note that in this figure, only the smooth, deterministic, velocity is shown.

the data where we used a smooth velocity model. In general, while the inversion returns estimated TDMT, the computed data does not resemble the observed data, regardless of the number of moment tensors we allowed in the solution. However the misfit, defined as the $L2$ difference between the predicted data and the actual data ($||\mathbf{Gm}-\mathbf{d}||_{L2}$) is smaller when we used all six independent terms in the moment tensor.

In general, the data misfit was relatively unaffected by the choice of the Green's functions that we used in the inversion. Specifically, we computed Green's functions for three cases: a smooth velocity model, a velocity model with a 1% stochastic variation in physical parameters, and a velocity model with a 2.5% stochastic variation. We inverted the data using the Green's functions computed using these three models, and computed the misfit for all cases (table 3.1. In general, allowing more moment tensor terms in the solution reduces the percent misfit, however, the computed data does not qualitatively resemble the observed data any better. The most likely reason for the poor misfit between the two is likely due to inaccuracies in the velocity models used to estimate the Greens functions. This is issue is compounded by the lack of quality timing information on the actual shot, which if known, could be used to constrain the velocity model.

**Table 3.1.** Summary of misfit, for three Green's functions estimates. The column on the left indicates which model was used to estimate the Green's functions. The norm of the misfit is indicated as $||\mathbf{Gm}-\mathbf{d}||$, as well as the percent misfit between the computed data ($\mathbf{Gm}$) and the observed data ($\mathbf{d}$).

| | 3 MT terms | | 6 MT terms | |
|---|---|---|---|---|
| % RMS stochastic variation | $\|\|\mathbf{Gm}-\mathbf{d}\|\|$ | % misfit | $\|\|\mathbf{Gm}-\mathbf{d}\|\|$ | % misfit |
| 0 | 0.004608 | 102.3 | 0.004275 | 70.5 |
| 1.0 | 0.004612 | 102.9 | 0.004272 | 70.3 |
| 2.5 | 0.004591 | 100.1 | 0.004246 | 68.6 |

In general, the estimated TDMT look reasonable in that the relative amplitudes of the on-diagonal terms seems appropriate. Also, we'd expect that the amplitudes of the off-diagonal TDMT terms to be significantly lower than the on-diagonal terms, which is what we observed in our our results, for both the time domain (Figure 3.14) and frequency domain (Figure 3.15). However, the off-diagonal terms in the TDMT are not zero, indicating that there is conversion of the P-wave energy that results from the explosion to convert into shear wave energy. This can be due to either (or both) near-source seismic scattering of $P$ wave energy to $S$ wave energy, or tectonic release of the numerous fractures that are known to exist in this area.

An encouraging result, albeit preliminary pending the development of an adequate velocity model, is that the frequency domain moment tensor estimates behave as expected (Figure 3.15), with regards to their relative spectral power. Over the primary frequency band of the data (2-10Hz), the amplitude of the absolute value of the frequency-domain moment tensor estimates are roughly two to three times higher for the on-diagonal terms than those of the off-diagonal terms. We also observe this behavior for f$<$1Hz, however, discount this as this frequency band is below the roll-off

for the instruments that we used.

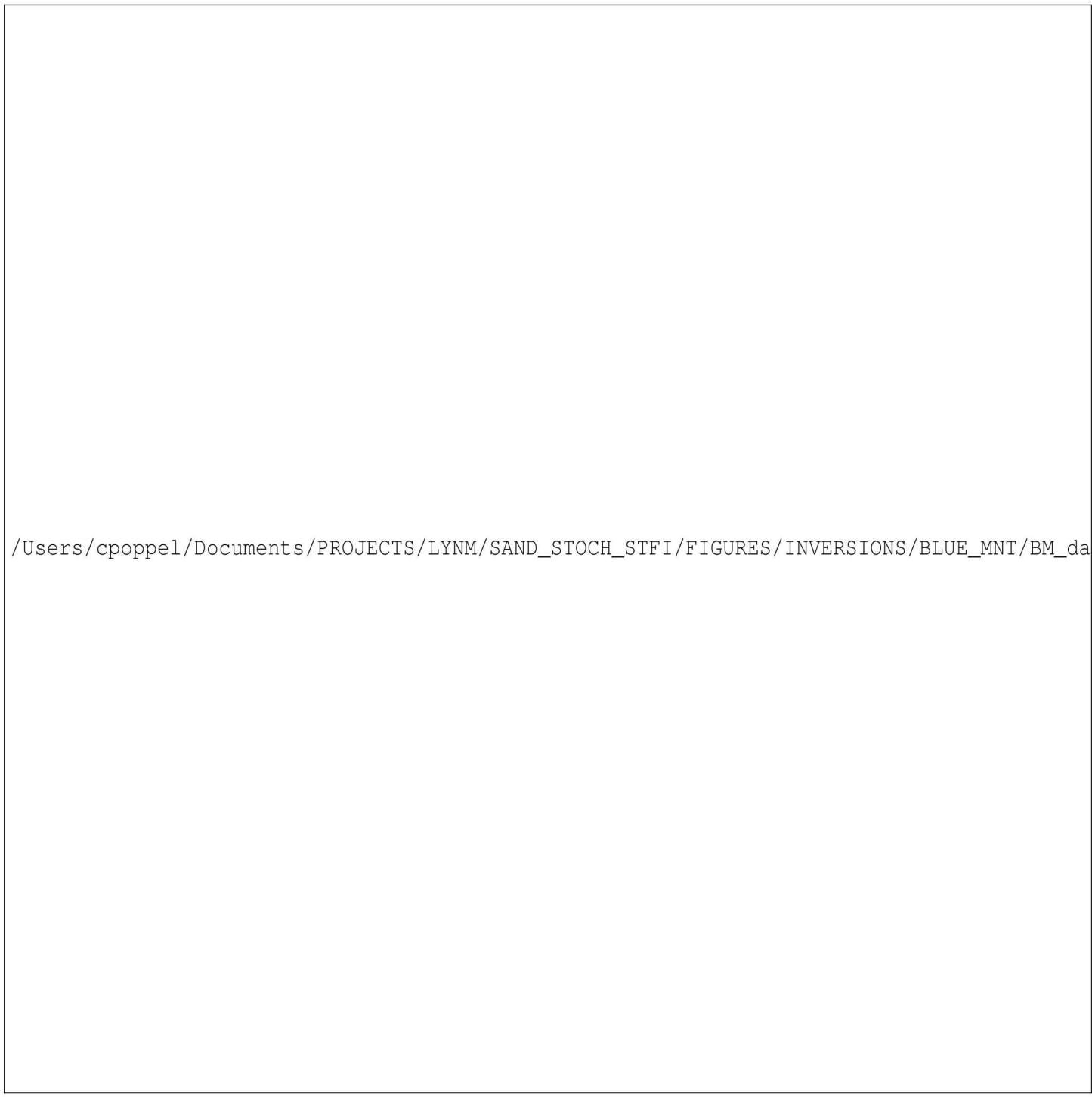


**Figure 3.12.** Ground velocity data from Shot 4 recorded by surface-located geophones. All the data shown here are used in the time-dependent moment tensor inversion. Amplitudes are trace normalized and the maximum amplitude for each seismogram is indicated in red above each trace.

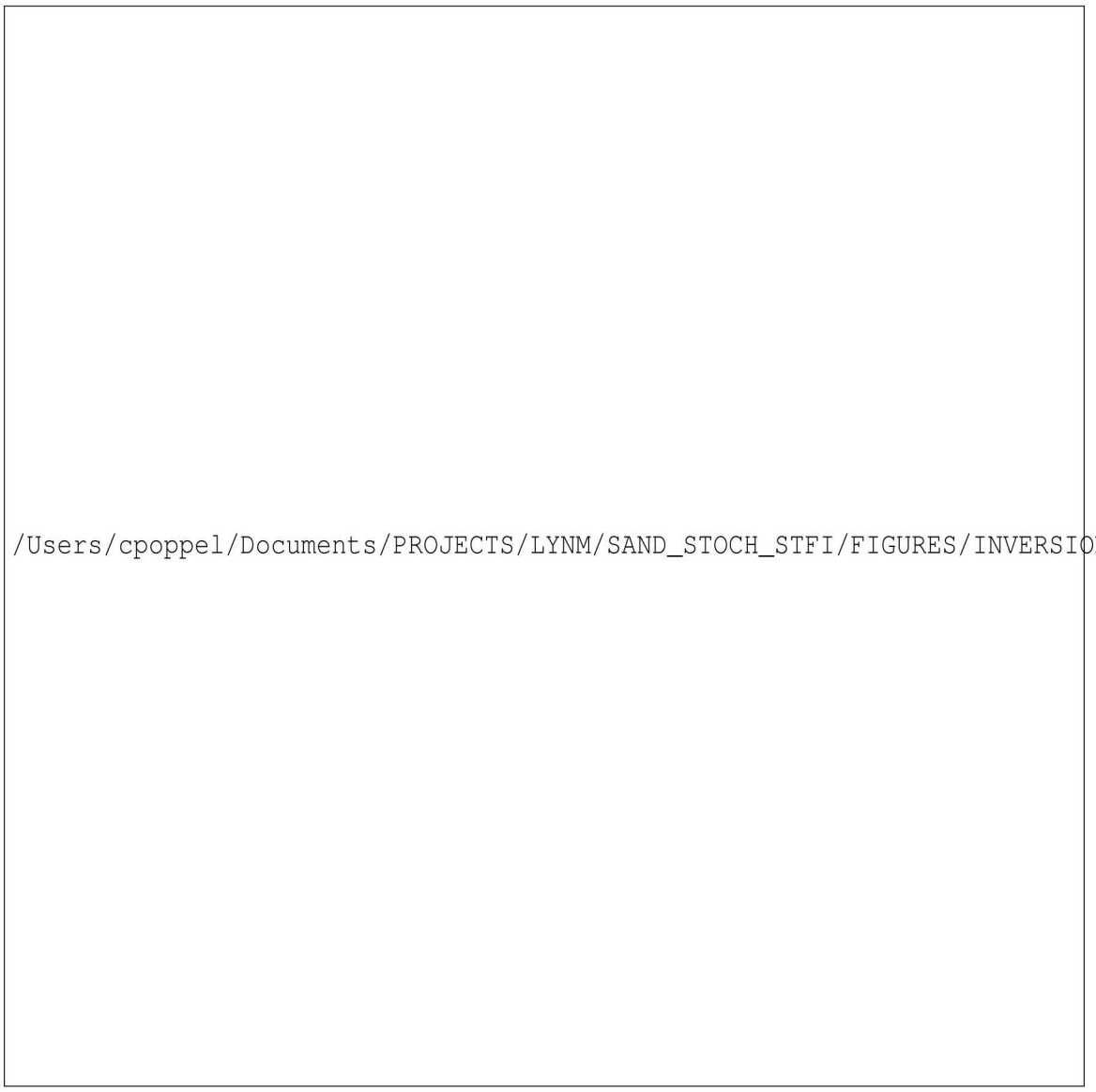


**Figure 3.13.** Inversion results, restricting the inversion to on-diagonal moment tensor terms. For these results, we used a smooth velocity model to estimate the Green's functions.

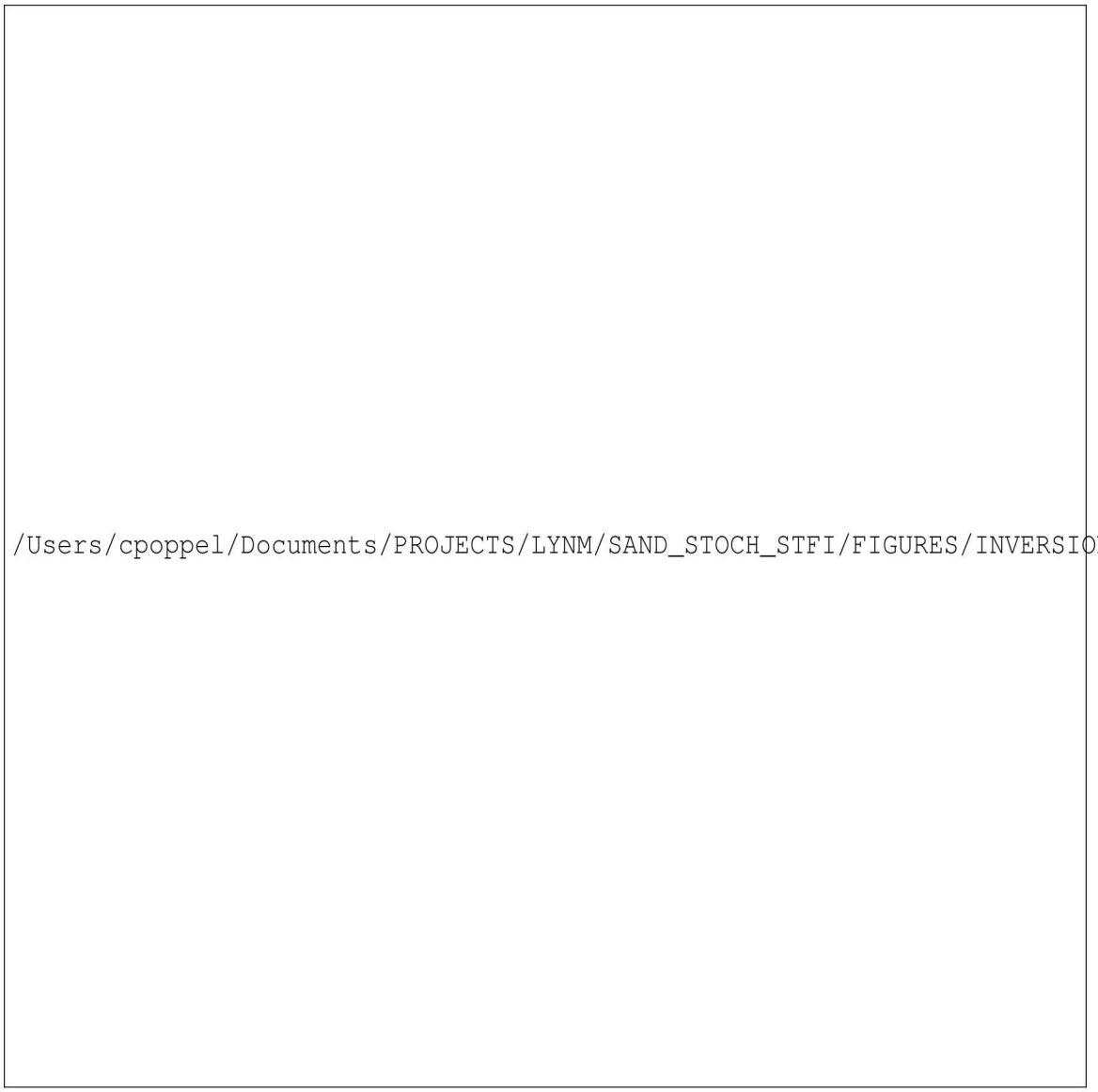


**Figure 3.14.** Inversion results, using the six independent moment tensor terms. For these results, we used a smooth velocity model to estimate the Green's functions.

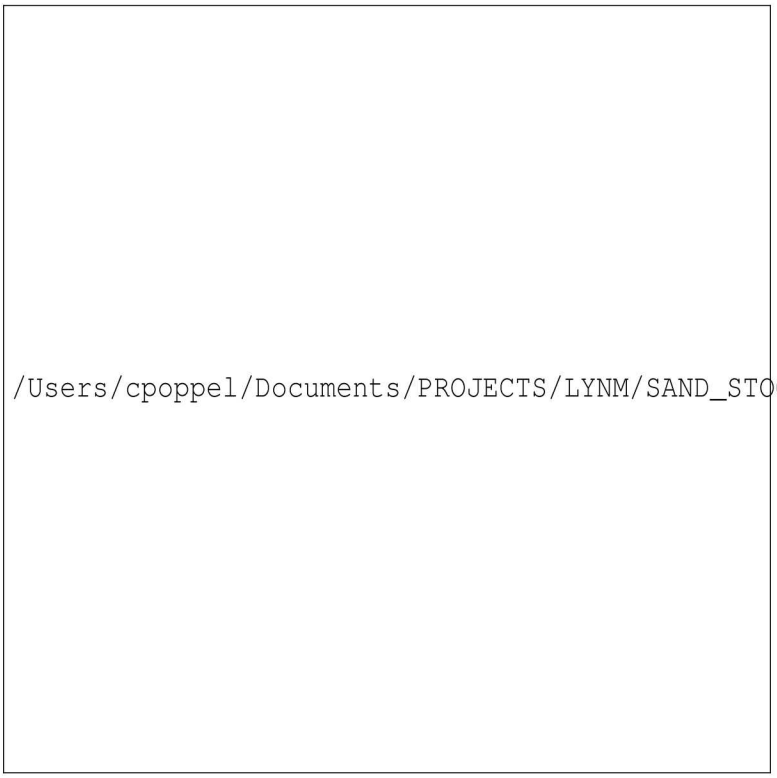


**Figure 3.15.** Frequency domain representation of the TDMT estimated in Figure 3.14. Note that the spectral power of the on-diagonal terms are significantly higher than the off diagonal terms, indicating that the source energy is primarily explosive.

# Chapter 4

# Summary

## 4.1 Summary

There were three primary goals of the work presented here. First, the development of a inversion method that could accurately and reliably estimate the seismic time dependent moment tensor. Our development is founded on a linear approximation and the simplification that the seismic source can be represented by a rank-2 tensor. However, we relax the assumption that all the terms on the moment tensor are required to posses the same time dependance. Specifically, we allow for all six independent terms in the moment tensor to independently vary in time, and refer to this as the time dependent moment tensor. The second major goal of this work we to introduce the concept of stochastic representations of geologic media. Although this idea is not new, we explored the effects of such materials in the context of moment tensor inversions using numerical experiments. Finally, we show the results of using our inversion scheme to estimate the TDMT of a single, subsurface explosion conducted as part of a well perforation procedure.

Numerical experiments validated the inversion scheme that we presented here. We were able to perfectly recover the TDMT for various source types using noise free synthetic data. We applied our inversion to a suite of source types, and so long as the Green's functions of the velocity model accurately reflected the characteristics of the velocity model used to construct the data, we were able to perfectly match the data. Predictably, when the assumed source mechanism designated in the inverse scheme did not reflect that used to construct the data, the misfit between the observed data and computed data increased.

One of the primary goals of the work here was to explore the effects of stochastic density/velocity perturbations in the geologic models. A stochastic Earthvelocity model is one that has a statistically defined variability in the density and/or velocity. Typically, the variability is only a fraction of the deterministic background density/velocity. We showed that even a small degree of stochastic variability can degrade the results of our inversion scheme. We saw that when the synthetic data was constructed using a velocity model with stochastic variation, unless the same exact model is used to estimate the Green's functions, the resulting estimated TDMT are quite affected. To illustrate this point, we computed synthetic data using a stochastic velocity model, but used Green's functions that were estimated using a smoothed version of the same velocity model. The inversion produced results that were degraded, in that the computed data did not match the observed data (Figure 3.8). This is not an unexpected result, however, we are not certain how to interpret future

results of our inversion. Perhaps statistical methods can be developed that will use an entire suite of stochastic models to estimate Green's functions, all of which can be used to invert a given data set. This is akin to Monte Carlo methods, and a topic of future research.

There is an important point to make regarding stochastic models in the context of waveform inversions: different realizations of a stochastic field will have identical power spectra. Given identical background velocity structure, the difference between one stochastic model and the next is only the phase of the stochastic field's spectrum. Therefore a better approach may be to estimate the moment tensor in the power spectral domain (e.g. Figure 3.15). As seen in Figures 3.7, 3.9, and 3.15 the power spectra of the estimated moment tensor are not as affected by inaccuracies of the stochastic variability. In these cases, the power spectra of the estimated moment tensor were similar despite using different Green's functions.

Our results of inverting the Blue Mountain data were less than satisfying. Specifically, our inversion did not appear to produce results that could explain the data. There are two likely reasons for this. First is that the velocity model that we used to estimate the Green's functions did not accurately reflect the geology of the site. Specifically, a seismic refraction survey shows clear evidence for a steeply dipping geologic boundary on the east side of the site. This boundary, the interface between bedrock and unconsolidated basin fill, presents a strong contrast in seismic velocities, which is not reproduced in our model. Furthermore, we have very little information on the gross 1D velocity structure of the site below depths of approximately 300m below ground surface. Recall that the shot depth was approximately 1000m below ground surface, which means that we have no geologic controls for the bottom 2/3 of the model. Because we did not have timing information on the shots, we could not use the travel time from the shot to the receivers to help constrain the velocity of the deeper portions of the model. The second likely reason for our poor results is that the data were quite noisy. To demonstrate this, we added random Gaussian noise to a synthetic dataset and inverted (Figure 4.1). At an approximately equivalent signal-to-noise ratio of our data (approximately 2-5), the synthetic test shows that quality of the estimated time dependent moment tensor terms is severely reduced.

## 4.2 Closing Remarks

We present a frequency-domain method of inverting seismic data for the time dependent moment tensor. Although the inversion method is not a new idea, our goals were primarily to start exploring the affects of stochastic variations in seismic velocity. Although we did not present an exhaustive investigation to this end, we did begin to explore some canonical models. We strongly encourage additional research into this subject, with deeper explorations into statistical analysis of Monte Carlo-like methods.

The inversion of the Blue Mountain seismic data was did not provide us with satisfactory results. This is based on the degree of misfit between the computed data and the observed data ($||\mathbf{Gm} - \mathbf{d}||$). We believe that this is primarily due to poor data quality, in terms of signal-to-noise, and a poorly constrained velocity model. Our next step in this problem is to produce a velocity

model that more accurately mimics the actual geology. We will need to incorporate the dipping interface between the low velocity basin fill material and much higher velocity bedrock. We will also need better constraints on the seismic velocities at depths greater than 300m, although its not yet clear how we will accomplish this. To reduce the deleterious effects of seismic scattering in our data, we may experiment with inversions at lower frequency bands, however, we are ultimately limited by the frequency band of the instruments which roll over at 4Hz.

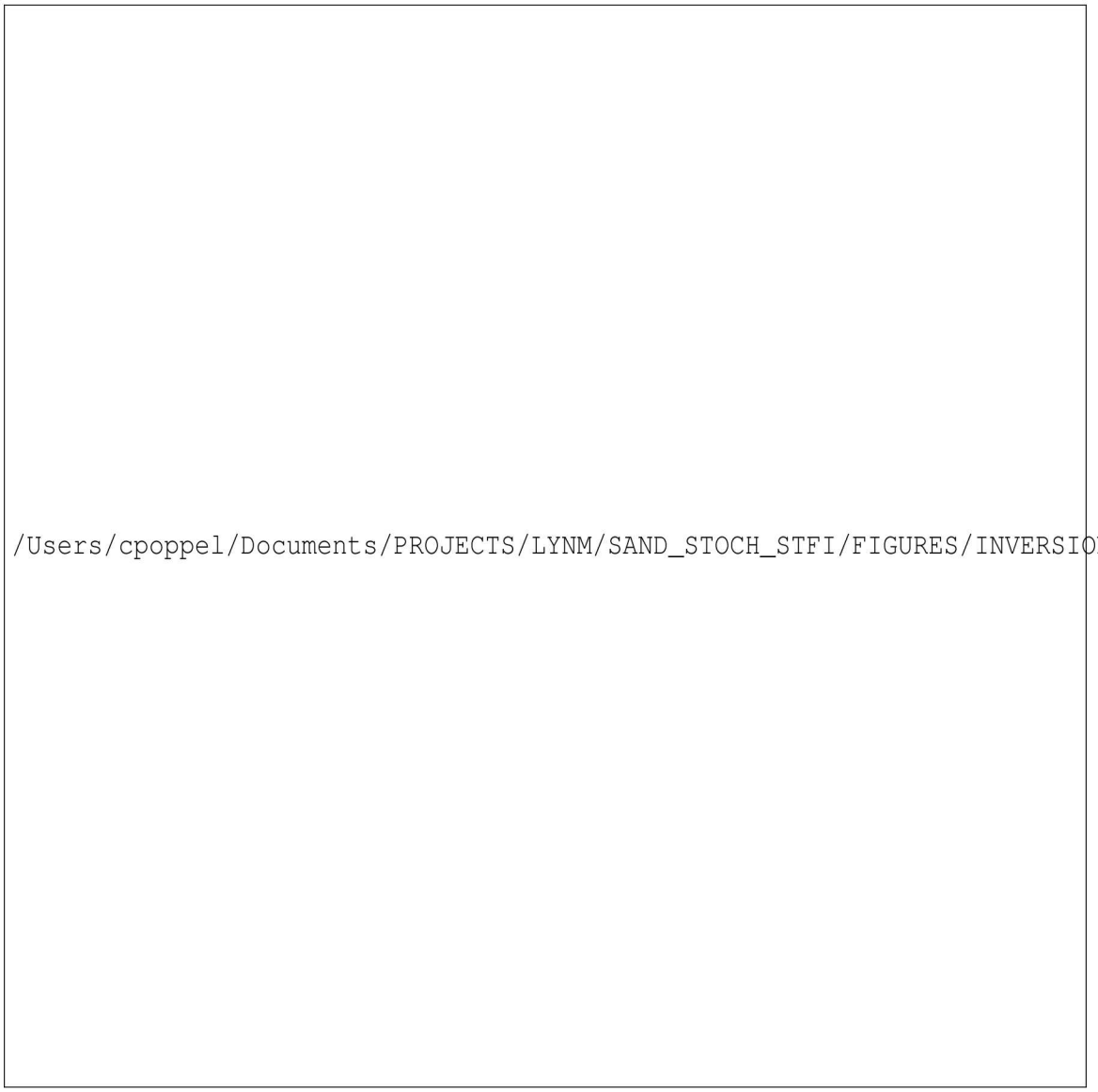


**Figure 4.1.** Inversion results for synthetic data, where we added Gaussian noise (filtered to 1-49Hz). The percentage number indicates the mean amplitude of the noise relative to the maximum amplitude of the data.

# Chapter 5

# References


Dahlen, F.A., and J. Tromp, 1998. Theoretical Global Seismology, Princeton University Press, Princeton, NJ.

Goff, J.A., Holliger, K., and A. Levander, 1994. Modal fields: a new method for characterization of random velocity heterogeneity, *Geophys. Res. Lett.*, **21**, 493-496.

Goff, J.A., and T.H. Jordan, 1988. Stochastic modeling of seafloor morphology: inversion foSea beam data for second-order statistics, *J. Geophys. Res.*, **93**, 13,589-13,608.

Holliger, K., A.R. Levander, 1992. A stochastic view of lower crustal fabric based on evidence from the Ivrea Zone, *J. Geophys. Res.*, **19**, 1153-1156.

Holliger, K., A.R. Levander, 1994 Structure and response of extended continental crust: stochastic analysis of the Stona-Ceneri and Ivrea zones, Italy, *Geology*, **22**, 79-82

Holliger, K., A. Levander, R. Carbonell, and R. Hobbs, 1994. Some attributes of wavefields scattered from Ivrea-type lower crust, *Tectonophysics*, **232**, 267-279.

Levander, A., England, R.W., Smith, S.K., Hobbs, R.W., Goff, J.A, and Holliger, K., 1994a. Stochastic characterization and seismic response of upper and middle crustal rocks based on the Lewisian gneiss complex, Scotland, *Geophys. J. Int.*, **119**, 243-259.

Levander, A., Hobbs, R.W., Smith, S.K., England, R.W., Snyder, D.B., and Holliger, K., 1994b. The crust as a heterogeneous 'optical' medium, or 'crocodiles in the mist', *Tectonophysics*, **232**, 281-297.

Poppeliers, C., 2007, Estimating vertical stochastic scale parameters from seismic reflection data: deconvolution with non-white reflectivity, *Geophys. J. Int*, bf 2(1), 769-778.

Poppeliers, C., 2009. Estimation of vertical continuous stochastic parameters from seismic reflection data, *Math. Geosci.*, **41**(7), 761-777.

Poppeliers, C., and A.R. Levander, 2004, Estimation of vertical stochastic scale parameters in the Earth's crystalline crust, *Geophys. Res. Lett*, **31**(13), doi.org/10.1029/2004GL019538.

Optim, Inc., 2007, Final Technical Report: Active Source Seismic Exploration and Development at the Blue Mountain Geothermal Project, Humboldt County, NV. Unpublished technical

report prepared by Optim, Inc. UNR, MS-174, 1664 N. Virginia Street, Reno, NV 89557.

Stein, S., and M. Wysession, 2003, An Introduction to Seismology, Earthquakes, and Earth Structure, Blackwell Publishing, LTD., Malden, MA.

Symons, N.P., D.F. Aldridge, D.H. Marlin, S.L. Collier, D.K. Wilson, and V.E. Ostashev, 2006, Staggered-Grid Finite-Difference Acoustic Modeling With the Time Domain Atmospheric Acoustic Propagation Suite (TDAAPS): Technical Report SAND2006-2540, Sandia National Laboratories.

# DISTRIBUTION:

| | | |
|---|---|---|
| 1 | MS MS0750 | Christian Poppeliers, 8861 |
| 1 | MS MS0750 | Leiph Preston, 8861 |
| 1 | MS MS0750 | Steven R Vigil, 8861 |
| 1 | MS MS0899 | Technical Library, 9536 (electronic copy) |
| 1 | MS 0899 | Technical Library, 9536 (electronic copy) |


Sandia National Laboratories